DOI: 10.1021/ma802705b

Macromolecules
ARTICLE

Self-Assembling Properties of Well-Defined Poly(ethylene oxide)-*b*-poly (ethyl acrylate) Diblock Copolymers

Sandie Piogé,[†,‡] Laurent Fontaine,[‡] Cédric Gaillard,[§] Erwan Nicol,[†,*] and Sagrario Pascual[‡]

[†]*Polymères, Colloïdes, Interfaces, UMR CNRS 6120, Université du Maine, Le Mans, France,* [‡]*Unité de Chimie Organique Moléculaire et Macromoléculaire, UMR CNRS 6011, Université du Maine, Le Mans, France, and* [§]*Laboratoire de Microscopie, plate-forme RIO BIBS, U.R. BIA, INRA, Nantes, France*

Received December 3, 2008; Revised Manuscript Received March 4, 2009

ABSTRACT: Poly(ethylene oxide)-*b*-poly(ethyl acrylate) amphiphilic diblock copolymers were synthesized by atom transfer radical polymerization (ATRP). The controlled character of the polymerization was confirmed by kinetic studies, evolution of number-average molecular weight and polydispersity index with conversion. Various block copolymers with different PEA/PEO molar ratio were synthesized and their self-assembling properties in aqueous medium were studied by fluorescence measurements, static light scattering (SLS), and dynamic light scattering (DLS). The critical micelle concentrations (CMC) were determined by pyrene fluorescence analysis. The CMC was shown to decrease as the hydrophobic (PEA) block length increases. SLS and DLS allowed the determination of the aggregation numbers (N_{agg}) and hydrodynamic radii (R_h) of the core−shell micelles formed in water. Both N_{agg} and R_h exhibit a monotonic increase as a function of the PEA block length. TEM and cryo-TEM micrographs of the micelles showed spherical objects with a low polydispersity of sizes. The micelles formed in water are in a thermodynamic equilibrium and the aggregation number of the micelles was shown to vary with the temperature.

Introduction

Amphiphilic block copolymers are well-known to self-assemble into micelles in selective solvent.[1,2] In the case of small solvophobic block copolymers, small spherical objects called star-like micelles are obtained. When the solvophobic block becomes much larger than the solvophilic one, "crew-cut" aggregates exhibiting various shapes (rods, worm-like, vesicles...) can be obtained.[3−7]

Poly(ethylene oxide) (PEO) is a water-soluble polymer that has been widely used as a nonionic hydrophilic block in many amphiphilic systems.[8] Because of its biocompatibility and low toxicity, PEO-based polymeric micelles have found interest in drug delivery materials.[9] Poly(ethylene oxide)-*b*-poly(propylene oxide) amphiphilic copolymers have been the most studied PEO-based surfactants because of their commercial availability. Triblock copolymers PEO-*b*-PPO-*b*-PEO form star-like micelles that can have biological applications[10] while PPO-*b*-PEO-*b*-PPO triblock form flower-like micelles and give hydrogels when their concentration increases.[11]

PEO-*block*-poly(meth)acrylates were the object of less studies than PEO-*b*-PPO or PEO-*b*-polystyrene. Various polymerization techniques have been used to polymerize acrylic monomers from functionalized PEO. Free radical polymerization, which is an unusual technique to obtain block copolymers, allowed the synthesis of PEO-*b*-poly(*n*-butyl acrylate).[12] Anionic polymerization has been applied to generate poly(*tert*-butyl acrylate) blocks.[13] However, the emergence of controlled/"living" radical polymerizations (CRP) in the past years has increased the chemical diversity of PEO-based block copolymers and also has simplified the synthesis in comparison to classical methods of living anionic polymerization. Moreover, CRP has allowed the synthesis of PEO-based block copolymers with predetermined molecular weights and narrow molecular weight distributions. Among CRP techniques, atom transfer radical polymerization (ATRP)[14,15] has proven to be a very versatile pathway for preparing amphiphilic copolymers based on PEO. The synthetic route used is a macroinitiator approach in which an hydroxy−PEO segment is transformed into an ATRP initiator. The latter can be obtained by coupling the hydroxy terminal functionality of PEO with either 2-bromopropionyl bromide or 2-bromoisobutyryl bromide. This approach has been used to synthesize amphiphilic block copolymers based on PEO and polyacrylates such as poly(ethyl acrylate) (PEA),[16,17] poly(*n*-butyl acrylate) (P*n*BA),[18] poly(*tert*-butyl acrylate) (P*t*BA)[17−19] and perfluorinated polyacrylates.[20] More complex macromolecular architectures have been elaborated from PEO and polyacrylates. Hou et al. synthesized star-block PEO_3-*b*-P*t*BA_3 and dendrimer-like PEO_3-*b*-P*t*BA_6 block copolymers, then, they hydrolyzed the P*t*BA block into poly(acrylic acid).[21] Kul et al. synthesized 5-arm star PEO_5-*b*-P*t*BA_5 by initiating the ATRP of *t*BA from a 5-arm PEO macroinitiator.[22] Durmaz et al. elaborated heteroarm H-shaped terpolymers by polymerizing *t*BA by ATRP and styrene by nitroxyde mediated polymerization (NMP) from a PEO "cross-bar" macroinitiator.[23]

This paper is the first step of a larger work which consists in elaborating more complex supramolecular architectures by cross-linking self-assembled systems. Cross-linked structures made of self-assembled block copolymers have a great potential of applications from medecine to microelectronics.[24,25] A few years ago, we reported the synthesis of polymerizable PEO-*b*-alkyl polymers and the photocross-linking of their star-like micelles in water.[26] However, the synthesis and the low aggregation numbers of micelles made of these copolymers limits the potentiality of elaborating new original macromolecular structures. Thus, we opted for polymerizable PEO-*b*-poly(ethyl acrylate)(PEA) copolymers, that are more adjustable and controllable systems. In the present work, we focused on the synthesis of PEO-*b*-PEA diblock

*Corresponding author. E-mail: erwan.nicol@univ-lemans.fr.

 Published on Web 05/08/2009

copolymers and the study of their self-associating properties in aqueous medium, the functionalization and cross-linking of the structures will be published later.

The synthesis of this PEO-*b*-PEA has already been reported by Dai et al.[16] and Ranger et al.[17] Both polymerized ethyl acrylate by ATRP from commercial PEO. However, the controlled radical polymerization of this monomer was not extensively described and the self-assembling properties of the corresponding block copolymers in water were not systematically studied as a function of the hydrophobic block length. This paper shows kinetic aspects of the ATRP of EA and brings a systematic study of the self-association properties of PEO-*b*-PEA as a function of the hydrophobic block length and the temperature.

Experimental Section

Materials. The PEO-monomethyl ether (M_w = 5000 g mol^{-1}) was purchased from Aldrich and contains 4% w/w of dihydroxy-telechelic chains (M_w = 10000 g mol^{-1}). It was dried by azeotropic distillation with toluene before use. Ethyl acrylate (EA, 99.5%) from Aldrich was distilled under reduced pressure and was stored at −18 °C after purification. Triethylamine (TEA, 99.5%) was distilled and stored over KOH prior to use. CuBr (99.999%), *N*,*N*,*N*′,*N*′,*N*″-pentamethyldiethylenetriamine (PMDETA, 99%), neutral alumina, diethyl ether, dichoromethane, and pyrene (99%) were purchased from Aldrich and were used without further purification. 4-(Dimethylamino)pyridine (DMAP, 99%) and 2-bromoisobutyryl bromide (99%) were used as received from Acros. The ligand Me_6Tren was prepared according to a reported procedure.[27]

Synthesis of PEO Macroinitiator. A 20 g (4.2 mmol) sample of PEO and 25 mg (0.2 mmol) of DMAP were dissolved in 400 mL of dry toluene. The solution was purged with nitrogen for 30 min and was cooled to 0 °C. TEA (1.75 mL: 12.6 mmol) and 2-bromoisobutyryl bromide (1.55 mL: 12.6 mmol) were added dropwise to the reaction mixture under continuous stirring. Then, the reaction was stirred for 48 h at 35 °C. The solution was filtered off and the solvent was removed under vacuum. The solid was dissolved in deionized water and the resulting solution was dialyzed for 3 days (cutoff membrane: 3500 g mol^{-1}) to remove low-molecular weight impurities. After dialysis, the solution was freeze-dried in order to recover the PEO macroinitiator.

Typical ATRP of Ethyl Acrylate Using a PEO Macroinitiator. In a Schlenk tube, a solution of 3.3 mL (0.03 mol) of ethyl acrylate, 3 g (0.6 mmol) of PEO macroinitiator and 12 mL (80% v/v) of toluene previously degassed by three freeze−pump−thaw cycles was added to another Schlenk tube containing 50 mg (0.3 mmol) of CuBr, under argon, with a cannula. The reaction mixture was degassed by three freeze−pump−thaw cycles and backfilled with argon. It was then placed in an oil bath thermostated at 50 °C. Then 63 μL (0.3 mmol) of PMDETA was added under argon (t = 0). After certain intervals, samples were withdrawn from the reaction mixture using a degassed syringe. Samples were dissolved in dichloromethane and were passed though a neutral alumina column in order to remove copper complex and were precipitated in a large excess of cold diethyl ether.

Size Exclusion Chromatography (SEC). Polymer molecular weights and polydispersity indices were determined using SEC on a system equipped with a SpectraSYSTEM AS100 autosampler, a column (JORDI gel 500 Å, 5 μm, 50 cm) followed by a Spectra Physics RI-71 refractive index detector and a Spectra Physics UV1000 detector (λ = 254 nm). THF was used as eluent at a flow rate of 1 mL/min at room temperature. The column was calibrated with the narrow molecular weight PEO standards (630−25000 g mol^{-1}).

NMR Spectroscopy. PEO macroinitiator and block copolymers were characterized by ^{1}H NMR, using a Brüker AC 400 MHz spectrometer and $CDCl_3$ as a solvent.

The molar composition of EA in the copolymer was determined by means of ^{1}H NMR spectroscopy (see Figure 2) from the integration area ratio of the signal originated from PEA block (H_e, OCH_2) at 4.15 ppm (excluding the signal of H_f at 4.2 ppm) and the signal characteristic from the PEO block (H_a, OCH_2) between 3.6 and 3.8 ppm according to the following equation:

$$f_{EA} = \frac{(I_e/2)}{(I_e/2) + (I_a/4)}$$

where I_a and I_e are the integration areas between 3.6−3.8 and 4.15 ppm, respectively.

Infrared. The FT-IR spectra were recorded on a Nicolet Avatar 370 DTGS spectrometer using the ATR accessory.

MALDI−TOF MS. Matrix-assisted laser desorption/ionization time-of-flight mass spectrometry was performed in the linear mode on a Bruker Biflex III apparatus equipped with a length of 120 cm. Dithranol was used as a matrix with accelerating potential of 19 kV.

Sample Preparation for Fluorescence Measurements. Samples for fluorescence measurements were prepared according to a procedure described elsewhere.[28] A 8.8×10^{-4} M stock solution of pyrene was prepared in dichloromethane. Then 20 μL of this solution was added to 20 mL empty vials in order to get a final pyrene concentration of 6.0×10^{-7} M for each sample. The dichloromethane was left to evaporate for 12 h in order to form a pyrene film in the vial. PEO-*b*-PEA block copolymer (0.1 g) was dissolved in 100 mL of Milli-Q water. This solution was filtered using inorganic membrane filter to 0.2 μm and used as a stock solution. This last one was diluted to obtain PEO-*b*-PEA solutions with concentrations ranging from 10^{-5} g/L to 10 g/L. Each solution was added to the vials containing pyrene, then, were heated at 60 °C for 4 h and stirred for 2 days at room temperature.

Fluorescence Measurements. Fluorescence spectra were recorded with a Horiba-Jobin Yvon fluorescence spectrophotometer in the right-angle geometry. For the fluorescence measurements, 3 mL of each sample were placed in a 1.0 cm square quartz cell. The emission spectra, were recorded using the excitation wavelength at 329 nm and the excitation spectra, were recorded using the emission wavelength at 371 nm. The widths of slits were set at 2 nm for both excitation and emission fluorescent measurements.

Light Scattering (LS). Static and dynamic light scattering were performed with a ALV-5000 multibit, multitau, full digital correlator in combination with a Spectra-Physics laser (emitting vertically polarized light at λ = 532 nm), and a thermostat bath controller (temperature control range: 10−90 °C). The autocorrelation functions were analyzed in terms of relaxation time (t) distribution. Measurements were made at angles of 40, 50, 70, 90, 110, and 130° at concentrations ranging from 1 to 10 g/L, and at 20 °C. Prior to measurement, the polymer solutions were filtered using inorganic membrane filter to 0.2 μm and were placed in a 20 mL flask previously cleaned using piranha solution (H_2O_2 (30%)/H_2SO_4 50/50 v/v); caution: piranha solutions are strongly oxidizing solutions and should not be stored in closed containers). The copolymer solutions are stable over months when stored at 4 °C in the dark.

The relative excess scattering intensity (I_r) was determined as the total intensity minus the solvent scattering divided by the scattering of toluene at 20 °C. I_r is related to the osmotic compressibility ($(d\pi/dC)^{-1}$) and the z-average structure factor (S(q)):[29,30]

$$I_r = KCRT(d\pi/dC)^{-1}S(q) \quad (1)$$

with R the gas constant and T is the absolute temperature.

$$K = \frac{4\pi^2 n^2}{\lambda^4 N_a}\left(\frac{dn}{dC}\right)^2\left(\frac{n_s}{n}\right)^2\frac{1}{R_s} \quad (2)$$

where N_a is Avogadro's number, dn/dC is the refractive index increment, and R_s is the Rayleigh ratio of toluene. $(n_s/n)^2$ corrects for the difference in scattering volume of the solution with refractive index n and toluene with refractive index: n_s. $R_s = 2.79 \times 10^{-5}$ cm $^{-1}$ at $\lambda = 532$ nm and 20 °C. $S(q)$ describes the dependence of I_r on the scattering wave vector: $q = (4\pi n/\lambda)\sin(\theta/2)$, with θ the angle of observation. For the systems studied here $S(q)$ was unity in the q-range covered by light scattering. The refractive index increment of the copolymer solutions is calculated from an expression established before[31]

$$\left(\frac{\mathrm{d}n}{\mathrm{d}C}\right) = W_{PEO}\left(\frac{\mathrm{d}n}{\mathrm{d}C}\right)_{PEO} + W_{PEA}\left(\frac{\mathrm{d}n}{\mathrm{d}C}\right)_{PEA} \quad (3)$$

where $(\mathrm{d}n/\mathrm{d}C)$, $(\mathrm{d}n/\mathrm{d}C)_{PEO}$, $(\mathrm{d}n/\mathrm{d}C)_{PEA}$ are the refractive index increments of the copolymer and the homopolymers PEO and PEA and W_{PEO} and W_{PEA} are the weight fractions of ethylene oxide et ethyl acrylate in the copolymer, respectively. The literature gives the values of $(\mathrm{d}n/\mathrm{d}C)_{PEO} = 0.135$ at $\lambda = 546$ nm at 20 °C in water[32] and of $(\mathrm{d}n/\mathrm{d}C)_{PEA} = 0.131$ at $\lambda = 546$ nm at room temperature in water.[33] In acetonitrile, one can find the values of $(\mathrm{d}n/\mathrm{d}C)_{PEO} = 0.135$ at $\lambda = 546$ nm at 20 °C,[32] and we measured, using a differential refractometer SpectraSYSTEM RI-150, the value of $(\mathrm{d}n/\mathrm{d}C)_{PEA} = 0.110$ for concentrations ranging from 1 to 3 g/L at 35 °C.

The normalized electric field autocorrelation function, $g_1(t)$, was calculated from the measured intensity correlation function, using the so-called Siegert relation.[34] $g_1(t)$ was analyzed in terms of a relaxation time (τ) distribution using the REPES routine:[35]

$$g_1(t) = \int A(\tau)\exp(-t/\tau)\,\mathrm{d}\tau \quad (4)$$

For all systems a fast q^2- dependent relaxation mode was observed caused by the relaxation of the concentration fluctuations of the micelles. The cooperative diffusion coefficient was calculated from the average relaxation rate as follows:

$$D_c = \langle\tau^{-1}\rangle/q^2 \quad (5)$$

Microscopy *TEM*. A drop of each aqueous dispersion specimen was first placed on a carbon-coated TEM copper grid (Quantifoil, Germany) and let to air-drying. The sample was then negatively stained with uranyl acetate (Merck, Germany). For that, the sample-coated TEM grid was successively placed on a drop of an aqueous solution of uranyl acetate (2% w/w) and on a drop of distilled water. The grid was then air-dried before introducing them in the electron microscope.

Cryo-TEM. Specimens for cryo-TEM observation were prepared using a cryoplunge cryo-fixation device (Gatan, USA) in which a drop of the aqueous suspension was deposited on to glow-discharged holey-type carbon-coated grids (Ted Pella Inc., USA). The TEM grid was then prepared by blotting the drop containing the specimen to a thin liquid layer remained across the holes in the support carbon film. The liquid film was vitrified by rapidly plunging the grid into liquid ethane cooled by liquid nitrogen. The vitrified specimens were mounted in a Gatan 910 specimen holder (Gatan, USA) that was inserted in the microscope using a CT-3500-cryotransfer system (Gatan, USA) and cooled with liquid nitrogen. TEM images were then obtained from specimens preserved in vitreous ice and suspended across a hole in the supporting carbon substrate.

All the samples were observed using a JEM 1230 "Cryo" microscope (JEOL, Japan) operated at 80 kV and equipped with a LaB_6 filament. For the cryo-TEM experiments, the microscope was operated under low dose conditions (< 10 e$^-$/A^2), at −178 °C. The micrographs were recorded on a Gatan 1.35 K × 1.04 K × 12 bit ES500W CCD camera.

Image Analysis. The software ImageJ (Research Services Branch NIMH & NINDS) has been used to determine particle size distributions and apply a contrast enhancement of the cryoTEM images.

Results and Discussion

1. Synthesis and Characterization of the Diblock Copolymers. The synthetic pathways of PEO−Br macroinitiator and PEO-*b*-PEA diblock copolymers are presented in Scheme 1.

PEO−Br macroinitiator was synthesized by reacting an hydroxyl-end-capped PEO with 2-bromoisobutyrate bromide in the presence of triethylamine (TEA) and 4-(dimethylamino)pyridine (DMAP) in toluene at 35 °C. The resulting macroinitiator was first characterized by FT-IR spectroscopy. Figure 1 reveals the representative FT-IR spectra of PEO, and the PEO−Br macroinitiator. The acylation of the hydroxyl-end group of PEO is shown by the appearance of a C═O (ester) band at 1731 cm^{-1}.

The chemical structure of the PEO−Br macroinitiator was also characterized by ^{1}H NMR spectroscopy. Figure 2b shows the appearance of two new signals at 1.94 ppm (labeled c) and at 4.25 ppm (labeled d) corresponding to two CH_3 of the bromoisobutyrate group and to the CH_2 of the EO unit adjacent to the ester group respectively. The integration area ratio of the -OCH_3 (labeled b) of the PEO chain end at 3.95 ppm and the CH_2 (labeled d) of the last EO unit at 4.25 ppm confirms the quantitative acylation of the hydroxyl-end group of the PEO.

The PEO−Br was also characterized by MALDI−TOF mass spectrometry: an envelope of the species can be observed, separated by 44.12 mass units corresponding to one EO unit (calculated value = 44.05) (Figure 3). An analysis of the peak values confirmed the reaction of hydroxyl-end-capped PEO with 2-bromoisobutyrate bromide. For example, the peak at $m/z = 4962.97$ is assigned to polymer chains with 108 EO units containing a sodium atom responsible for ionization, and bromoisobutyrate group as the chain end (calculated value = 4961.43).

Scheme 1. Synthesis Route of PEO-*b*-PEA Block Copolymers[a]

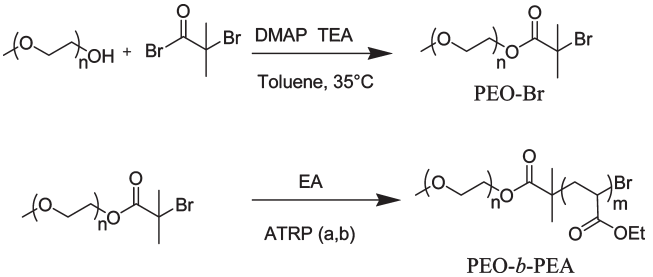

[a]Key: (a) $[EA]_0$:$[POE\text{-}Br]_0$:$[Cu(I)Br]_0$:$[PMDETA]_0$ = 25:1:0.5:0.5, toluene (80% v/v), 50 °C; (b) $[EA]_0$:$[POE\text{-}Br]_0$:$[Cu(I)Br]_0$:$[Me_6TREN]_0$ = 25:1:0.1:0.1, toluene (80% v/v), 30 °C.

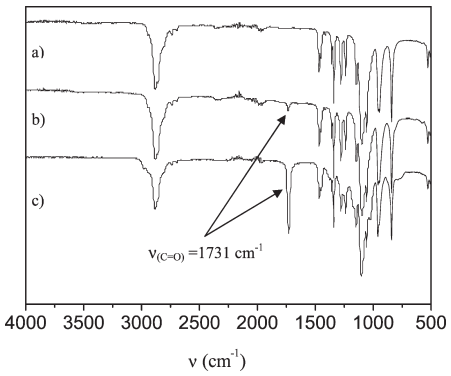

Figure 1. FT-IR spectra of (a) PEO, (b) PEO−Br, and (c) PEO-*b*-PEA_{17}.

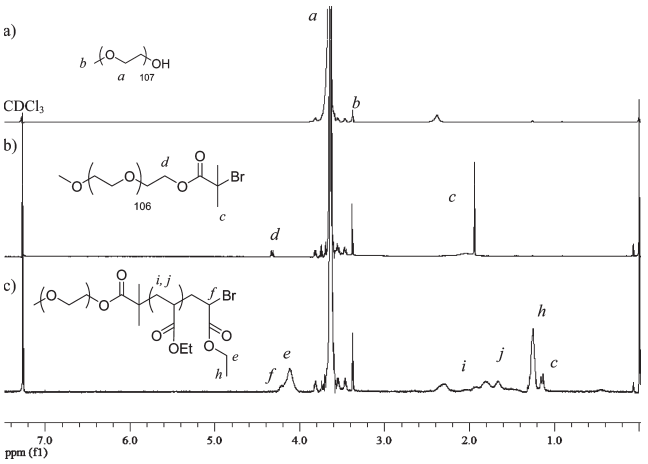

Figure 2. ^{1}H NMR spectra of (a) PEO, (b) PEO−Br, and (c) PEO-*b*-PEA_{10} in $CDCl_3$.

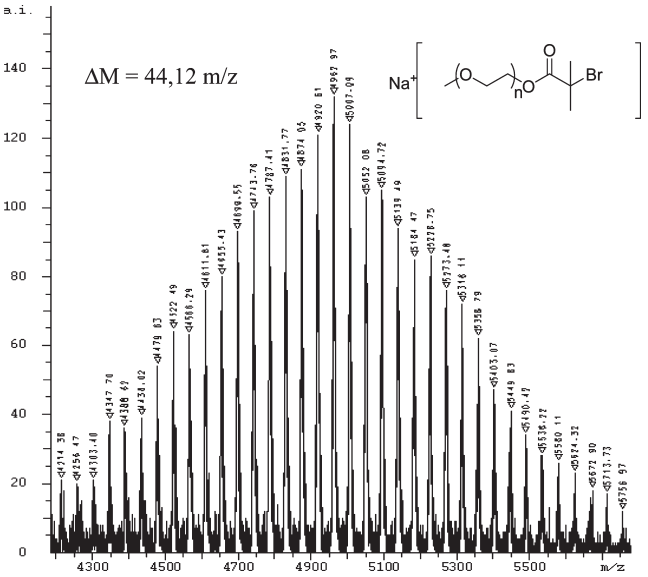

Figure 3. MALDI−TOF MS spectrum (linear mode, matrix = dithranol) of PEO−Br macroinitiator.

The PEO−Br macroinitiator was engaged in copper-mediated ATRPs of EA with Cu(I)Br/PMDETA and Cu(I)Br/Me_6TREN catalytic systems at 50 °C and at room temperature, respectively (Scheme 1). The linear amine PMDETA[36] and the Me_6TREN[37] are ligands commonly used to afford good control of acrylates polymerizations. Experiments were carried out in toluene (80% v/v) using monomer/initiator ratio of 25/1. Plots of $\ln([M]_o/[M]_t)$ versus time (Figure 4) are linear with both catalytic systems showing first-order kinetics compatible with a constant concentration of active species. A faster rate of polymerization is observed using Cu(I)Br/Me_6TREN. This result is in accordance with the work reported that the general order of activation rate constant of Cu complex for amine ligand is tetradentate > tridentate > bidentate.[38]

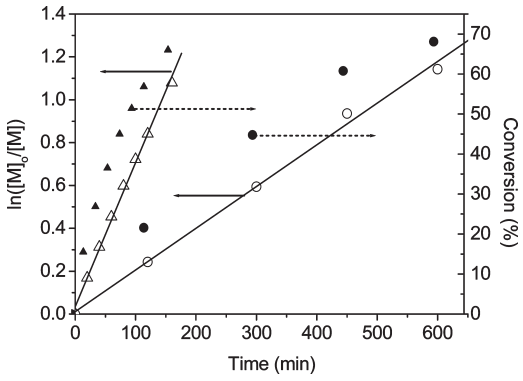

Figure 4. Kinetic plots for the ATRP of ethyl acrylate in 80% v/v of toluene using PEO−Br as macroinitiator, different ligands and different temperatures. (▲, △) $[EA]_0$:$[POE\text{-}Br]_0$:$[Cu(I)Br]_0$:$[Me_6TREN]_0$ = 25: 1: 0.1: 0.1 at 30 °C; (●, ○) $[EA]_0$:$[POE\text{-}Br]_0$:$[Cu(I)Br]_0$:$[PMDETA]_0$ = 25: 1: 0.5: 0.5 at 50 °C.

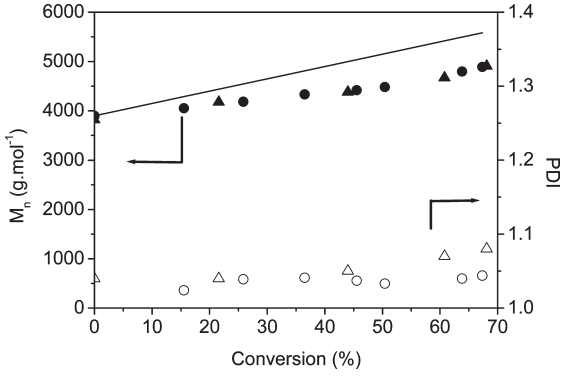

Figure 5. Evolution of number average molecular weights (filled symbols) and of polydispersity indices (open symbols) for the ATRP of ethyl acrylate in 80% v/v of toluene using PEO−Br as macroinitiator, different ligands and different temperatures. (▲, △) $[EA]_0$:$[POE\text{-}Br]_0$:$[Cu(I)Br]_0$:$[Me_6TREN]_0$ = 25:1:0.1:0.1 at 30 °C; (●, ○) $[EA]_0$:$[POE\text{-}Br]_0$:$[Cu(I)Br]_0$:$[PMDETA]_0$ = 25:1:0.5:0.5 at 50 °C. The straight line corresponds to the theoretical molecular weight.

The plots of number-average molecular weight versus conversion (Figure 5) show a good agreement between experimental values and theoretical ones, and polydispersity indices values remain low (1.03 −1.08). All of the experimental criteria of a controlled polymerization shown in these experiments proved the efficiency of both catalytic systems (Cu(I)Br/PMDETA and Cu(I)Br/Me_6TREN) in the copper-mediated ATRP of ethyl acrylate.

As seen in Figure 1, the FT-IR spectrum of PEO-*b*-PEA_{17} block copolymer (Table 1) exhibits a band at 1731 cm^{-1}, assigned to the carbonyl absorption of PEA block, which is much stronger than that of PEO−Br macroinitiator. Figure 2c shows the ^{1}H NMR spectrum of a PEO-*b*-PEA_{10} diblock copolymer (Mn_{SEC} = 4400 g/mol, PDI = 1.05). The presence of broad peaks between 4.0 and 4.3 ppm and 1.2−2.4 ppm due to respectively, the OCH_2 (labeled e) and to the CH_3, CH and CH_2 (labeled h, i, j) of the EA units illustrates the presence of PEA block in the final polymer. Thus, the chemical structure of PEO-*b*-PEA_{10} diblock copolymer (Table 1) was confirmed by ^{1}H NMR spectroscopy.

Table 1. Molecular Characteristics of PEO-*b*-PEA Block Copolymers and Their Precursor

	M_n (kg·mol^{-1})						molar composition	
samples	SEC[a]	^{1}H NMR	M_{peak} (kg·mol^{-1}) MALDI−TOF	M_w (kg·mol^{-1}) SLS	PDI[a]	DP[b] EA	PEO	PEA
PEO	3.8	4.7	4.7	4.2	1.03		1	0
PEO−Br	3.9	4.8	4.9		1.04		1	0
PEO-*b*-PEA5		5.3	5.6			4.8	0.96	0.04
PEO-*b*-PEA7		5.5		5.0	1.05	6.8	0.94	0.06
PEO-*b*-PEA8	4.3	5.6			1.05	8.5	0.93	0.07
PEO-*b*-PEA10	4.4	5.9	5.9	5.3		10.4	0.91	0.09
PEO-*b*-PEA12	4.5				1.04	12.4	0.90	0.10
PEO-*b*-PEA17	4.8	6.6	6.4	5.9	1.05	17.0	0.86	0.14
PEO-*b*-PEA21	5.0	6.9		6.6	1.08	20.7	0.84	0.16
PEO-*b*-PEA25	5.3	7.3	7.4	6.8	1.06	24.9	0.81	0.19
PEO-*b*-PEA32	5.7	8.0			1.07	31.7	0.77	0.23

[a] Determined by SEC using poly(ethylene oxide) standards. [b] Determined by ^{1}H NMR spectroscopy.

Figure 6 presents the SEC traces of PEO−Br macroinitiator and PEO-*b*-PEA$_{25}$ block copolymer. The SEC trace of the block copolymer shows no detectable quantity of unreacted macroinitiator, indicating a high initiating efficiency of the PEO−Br macroinitiator. The peak at low elution volume, in both cases, corresponds to the difunctional PEO chains having twice the molar mass of the monofunctional PEO. The shift of this peak after ATRP indicates also a quantitative functionalization of these macromolecules.

The ATRP of ethyl acrylate using PEO−Br as a macroinitiator using Cu$^{(I)}$Br/PMDETA and Cu$^{(I)}$Br/Me$_6$TREN as catalytic systems in toluene (80%v/v) have proven to be versatile pathways to synthesize well-defined PEO-*b*-PEA block copolymers. As PMDETA is a commercial ligand, several block copolymers with a large range of molar compositions have been synthesized using Cu^{I}Br/PMDETA as catalytic system in toluene (80% v/v) at 50 °C. The number-average molecular weights, polydispersity indices and molar compositions of block copolymers, are gathered in Table 1. All copolymers showed narrow molecular-weight distributions. The PEA block lengths range from 5 to 32 repeat units, corresponding to 4−23 molar percent in the copolymers.

2. Self-Assembly in Aqueous Solution. *2.1. Determination of the Critical Micelle Concentration (CMC) of PEO-b-PEA.* The onset of micelle formation of our amphiphilic block copolymers was evaluated using steady-state fluorescence spectroscopy of pyrene. The photophysical properties of pyrene are known to be strongly dependent on the polarity of its environment.[39] This feature has allowed using this fluorophore as a probe to determine critical micelle concentrations (CMC) for many nonionic and ionic amphiphilic block copolymers[28,40−50] or polysoaps[51] in aqueous solutions.

Typical emission and excitation spectra of aqueous solutions of pyrene and PEO-*b*-PEA block copolymers at various concentrations are shown in Figure 7. When the environment of pyrene changes from polar to nonpolar, both emission and excitation spectra are altered. In the pyrene excitation spectra, the first vibronic band (0,0) in water shifts from 333.5 to 336.5 nm as the copolymer concentration increases. This distinct shift provides evidence for a transfer of pyrene probe from a polar environment to an apolar one and thus provides information on the location of the pyrene probe in the system (in water or in micelles cores).

The intensity ratio of the excitation bands at 336.5 and 333.5 nm ($I_{336.5}/I_{333.5}$) for copolymers bearing PEA blocks of various lengths are shown in Figure 8. Typical sigmoidal shapes are observed and the $I_{336.5}/I_{333.5}$ ratio varies from 0.4 to 0.6, when pyrene is in a polar environment, to 1.4−1.5 when it is located in the micelles cores. It should be pointed out that the polarity variation probed by the pyrene ranges over two decades of concentration indicating a very weak cooperativity of the macromolecules association.

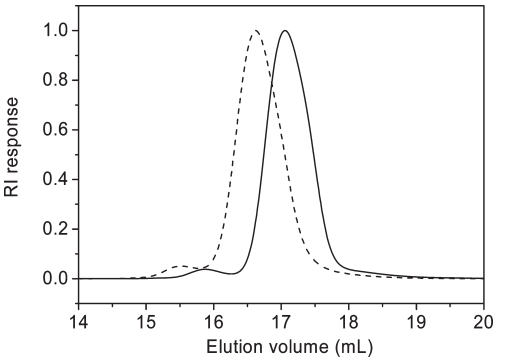

Figure 6. SEC traces of PEO−Br macroinitiator (solid line) and PEO-*b*-PEA$_{25}$ block copolymers (dashed line).

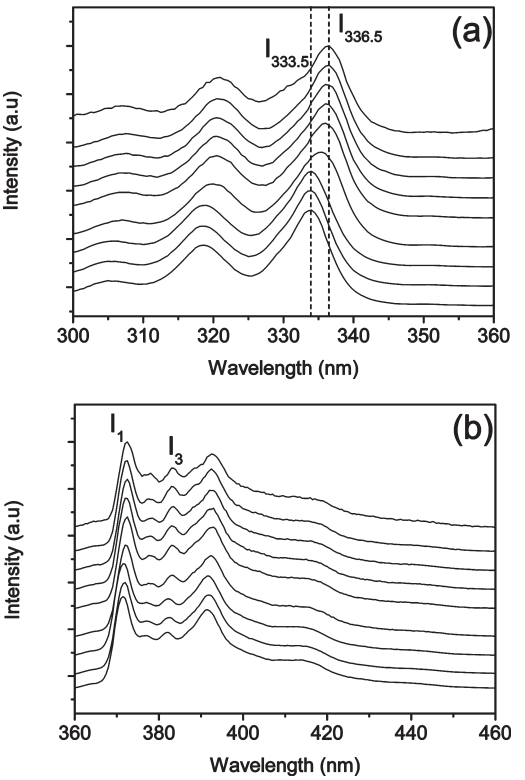

Figure 7. Excitation (a) and emission (b) spectra of pyrene solutions in the presence of PEO-*b*-PEA$_{12}$. From bottom to top, concentration of copolymer ranges from to 0.0001 to 9.8 g L^{-1}.

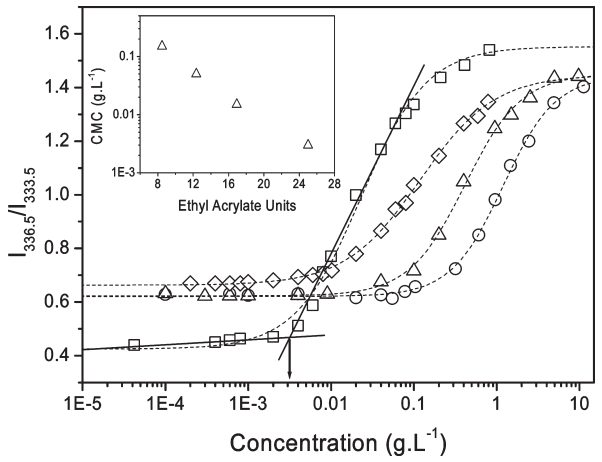

Figure 8. Fluorescence intensity ratio $I_{336.5}/I_{333.5}$ (from pyrene excitation spectra) as a function of concentration for (○) PEO-*b*-PEA$_8$, (△) PEO-*b*-PEA$_{12}$, (◇) PEO-*b*-PEA$_{17}$, and (□) PEO-*b*-PEA$_{25}$. Dashed lines are guides to the eyes. The solid lines give an intercept that allows the estimation of the critical micelle concentration (arrow). The inset shows the evolution of the CMC as a function of the ethyl acrylate block length in a semilogarithmic representation.

Wilhelm et al. have shown that the variation of the intensity ratio ($I_{336.5}/I_{333.5}$) was due to both the self-association of the amphiphilic molecules and the partition of pyrene between the aqueous phase and the micelles cores.[28] They concluded that the apparent concentration, taken as the intersection of the tangents to the curve at the inflection point at low concentration (see Figure 8), was always larger than the real critical micelle concentration. Our purpose was not to determine the CMC with a very high accuracy and we satisfied with the estimation of the CMC given by the tangent method. The values of apparent CMC are gathered in Table 2. The CMC determined in the present work are a little bit lower than those measured by Dai et al.[16] for similar block copolymers. Indeed, they found a CMC around 0.04 g L^{-1} for a PEO$_{100}$-*b*-PEA$_{10}$ while, according to Figure 8, we expect a value around 0.1 g L^{-1} for the same block copolymer.

The inset in Figure 8 exhibits a monotonic decrease of the apparent CMC as a function of the hydrophobic block length in a semilogarithmic scale. This evolution was expected and the same behavior has already been shown with poly(alkylene oxide) block copolymers in water[52] or PS-*b*-poly(acrylic acid) in organic solution.[53]

2.2. Light Scattering Measurements. Static light scattering (SLS) provides information on the time-averaged properties of the system. The apparent weight-averaged molecular weight (M_w) can be obtained by the Debye relationship:

$$\frac{KC}{I_r} = \frac{1}{M_w}\left(1 + \frac{R_g{}^2 q^2}{3}\right) + 2A_2C \qquad (6)$$

where C is the concentration (in g/L), I_r is the relative excess scattering intensity, K gathered the optical parameters, R_g is the radius of gyration, q is the scattering wave vector, and A_2 is the second virial coefficient.

The weight averaged molar mass M_w were obtained by extrapolating KC/I$_r$ values to $q = 0$ and $C = 0$ according to eq 6. M_w of the copolymers in water are listed in Table 2. The values of M_w are substantially larger than those corresponding to the unimers, determined in acetonitrile (good solvent for both blocks) (see Table 1), indicating the aggregation of PEO-*b*-PEA into micelles in aqueous solutions. The average aggregation number N_{agg} of PEO-*b*-PEA in aqueous solution is calculated according to the following equation:

$$N_{agg} = \frac{\overline{M}_{w(micelle)}}{\overline{M}_{w(unimer)}} \qquad (7)$$

where $\overline{M}_{w(micelle)}$ and $\overline{M}_{w(unimer)}$ are the weight-average molecular weight of the micelles (measured in water) and of the single block copolymer chain (measured in acetonitrile), respectively.

Table 2. Micellar Properties from Fluorescence Measurements, Static and Dynamic Light Scattering

sample	apparent CMC (g L^{-1})	M_w micelles (kg·mol^{-1})	N_{agg}	R_h (nm)[a]
PEO-*b*-PEA5		65.0	13	8.5 ± 0.3
PEO-*b*-PEA8	0.15	92.6	18	9.7 ± 0.3
PEO-*b*-PEA10		184.8	35	9.9 ± 0.5
PEO-*b*-PEA12	0.05	253.0	48.8	11.2 ± 0.2
PEO-*b*-PEA17	0.015	365.0	62	11.4 ± 0.3
PEO-*b*-PEA21		438.0	66	12.3 ± 0.3
PEO-*b*-PEA25	0.003	1282.0	111	15.0 ± 0.3

[a] The error bar is the deviation to the mean value measured at different detection angles by DLS.

Three different ways of preparing the block copolymers samples in water were investigated. A target concentration was obtained by (a) dissolving the copolymer powder in water at the desired concentration, (b) preparing a highly concentrated solution then diluting it, and (c) dissolving the copolymer in THF (good solvent of both blocks), adding water slowly and then evaporating the cosolvent. All these preparation routes lead to the same micellar structure (same aggregation number and hydrodynamic radius). It has been shown that, in the case of kinetically frozen micellar systems, the structure of micelles depends on the preparation route.[54,55] Thus, this could indicate that PEO-*b*-PEA block copolymers form micelles that are in thermodynamic equilibrium. Different ways seem to lead to dynamical self-assembled structure: Bendejacq et al. showed that introducing hydrophilic monomer units in the hydrophobic block can induce a dynamical character to the self-assembly.[56] The works of Eisenberg's team showed that PS-*b*-PAA crew-cut aggregates can be dynamical when solvent mixtures are used.[57,58] At last, we believe that highly asymmetric copolymers bearing small hydrophobic blocks could lead to micelles in thermodynamic equilibrium. This feature is well-known for associative polymers bearing alkyl[59] or perfluoroalkyl moieties.[60]

As shown in Figure 9, the micellar number of micelles increases monotonically as the hydrophobic block length increases. A theory developed by Halperin[61] predicts a power law dependence of the aggregation number with hydrophobic block length (N_B): $N_{agg} \propto N_B{}^{4/5}$. Noolandi and Hong[62] found the aggregation number to scale as $N_{agg} \propto N_B{}^{0.9}$. Nagarajan et al.[63] calculated for PEO-*b*-PPO in water the scaling equation $N_{agg} \propto N_B{}^{1.19} N_A{}^{-0.51}$ (where N_A is the degree of polymerization of the PEO block). By plotting $\log(N_{agg}) = f(\log(N_B - N_{Bcr}))$ (where N_{Bcr} is the critical hydrophobic length for micelle formation), experimental measurements obtained by Booth et al.[64] give the exponents of 0.98 for PEO-*b*-PPO, 1.17 for PEO-*b*-PBO and 0.83 for PEO-*b*-poly(styrene oxide). Other block copolymers, not based on PEO, have been studied in organic solvent or in solvent mixtures. Antonietti and Förster studied polystyrene-*b*-poly(4-vinylpyridine) (PS-*b*-4PVP) in organic selective solvents of the PS block.[65,66] They found that N_{agg} scales with N_{4PVP} with an exponent varying from 1.5 to 2 depending on the solvent used. Their results are in agreement with the theory that predicts $N_{agg} \propto N_B{}^2$ assuming that the micelle

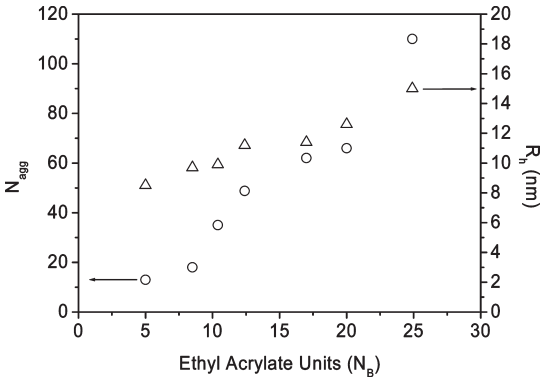

Figure 9. Evolution of the average aggregation number (circles) and hydrodynamic radius (triangles) of micelles as a function of the hydrophobic block length.

core is strongly segregated and behaves like a gel-like polymer droplet. Qin et al. found similar results with polystyrene-*b*-poly(methacrylic acid) (PS-*b*-PMA) in dioxane/water mixtures.[67] For diblock copolymers, $N_{agg} \propto N_{ps}^{1.89} N_{PMA}^{-0.86}$ and for triblock copolymers, $N_{agg} \propto N_{ps}^{1.62} N_{PMA}^{-0.41}$. These exponents are much larger than those found for PEO based materials. A possible explanation could be that PEO based copolymers form less strongly segregated core micellar structures. We can also wonder about the equilibrium state of very strongly segregated aggregates and its influence on the aggregation number. Very different results were obtained by Khougaz et al. on PS-*b*-PAA and PS-*b*-PANa (sodium acrylate form) copolymers in organic solvent. They found the relation $N_{agg} \propto N_{PANa}^{0.5} N_{PS}^{-0.6}$. However, the N_{PANa} dependence varies with the PS block length and with solvent used. It should be pointed out that the solvophobic blocks are very small (from 2.6 to 21 units) in this study and that all of the chains are not micellized for the shortest PANa blocks.

In the present study, the scaling relation gives $N_{agg} \propto N_{EA}^{1.34}$. This exponent is surprisingly high compared to the values found in the literature for poly(alkylene oxide) based block copolymers. However, a very small range of ethyl acrylate block lengths (less than one decade) is covered in our work and the exponent value could be overestimated because of the short EA block length. Considering only the copolymers bearing PEA blocks larger than 10 units, the scaling law gives an exponent value of 1.09, suggesting that, weakly hydrophobic copolymers behavior cannot be well described by the theories. The theories assume the micelle core to be fully segregated and devoid of solvent. The disagreement between the prediction and the experimental data suggest that PEO-*b*-PEA micellar cores could be partially hydrated because it seems unreasonable to assume a stronger segregation of the micelle cores for the smallest PEA blocks.

The hydrodynamic radius R_h of unimers and micelles were determined from dynamic light scattering (DLS) by calculating the diffusion coefficient using the Stokes−Einstein relation:

$$D = \frac{kT}{6\pi\eta R_h} \tag{8}$$

Here η is the viscosity of the medium (water or acetonitrile), T the absolute temperature, and k the Boltzmann constant. Note that no q-dependence of the diffusion coefficients was observed. The hydrodynamic radius of PEO-*b*-PEA unimers, in acetonitrile, was around 2−3 nm as expected. DLS analyses of the aqueous solutions of PEO-*b*-PEA show a linear increase of R_h with the PEA length (see Figure 9).

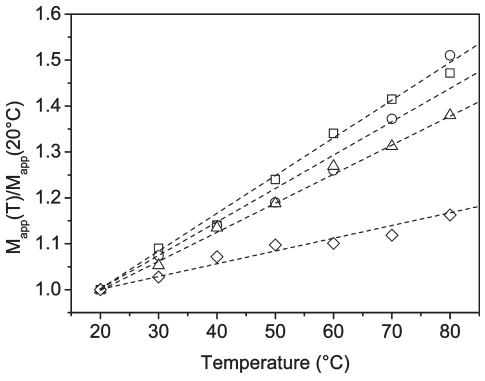

Figure 10. Temperature dependence of the apparent molar mass at the temperature (T) normalized by its value at 20 °C for PEO-*b*-PEA_8 (□), PEO-*b*-PEA_{10} (○), PEO-*b*-PEA_{12} (△) and PEO-*b*-PEA_{17} (◇). Dashed lines are guides to the eye.

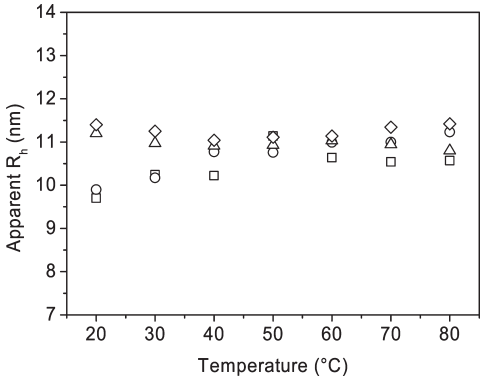

Figure 11. Temperature dependence of the apparent hydrodynamic radius of PEO-*b*-PEA_8 (□), PEO-*b*-PEA_{10} (○), PEO-*b*-PEA_{12} (△) and PEO-*b*-PEA_{17} (◇)

It must be pointed out that the hydrodynamic radius is larger than expected. A rough calculation of the core size can be made by comparison with the end-capped PEO_{5k}-alkyl studied by Renou et al.[68] We assume that the PEO corona, in PEO_{5k}-*b*-PEA, have the same size than in the case of end-capped PEO_{5k}-octadecyl for an equivalent aggregation number. In this system, the octadecyl groups are in a bulky state; the core size can be calculated according to the following equation:

$$R_{core} = \left[\frac{3N_{agg}M_{C18}}{4\pi N_a \rho}\right]^{1/3} \tag{9}$$

Here, M_{C18} is the molar mass of the octadecyl group (253 g mol^{-1}), N_a is Avogradro's number, and ρ is the specific volume (0.78×10^{-21} g.nm^{-3}).

A value of R_h = 1.6 nm is found for the octadecyl core. Renou et al.[68] measured 7.9 nm for the hydrodynamic radius of micelle having an aggregation number of 36. The thickness (δ_{corona}) of the corona has been, thus, estimated to 6.3 nm. The closest aggregation number can be found for PEO-*b*-PEA_{10} copolymer (N_{agg} = 35). The core size can be estimated by the way, assuming a bulky state, according to the following equation:

$$R_{core} = \left[\frac{3N_{agg}M_{EA}\mathrm{DP}_{EA}}{4.\pi N_a \rho}\right]^{1/3} \tag{10}$$

Here, M_{EA} is the molar mass of the ethyl acrylate unit (100.1 g mol^{-1}), DP_{EA} is the degree of polymerization, and ρ is the specific volume of the PEA ($1.12.10^{-21}$ g nm^{-3}).

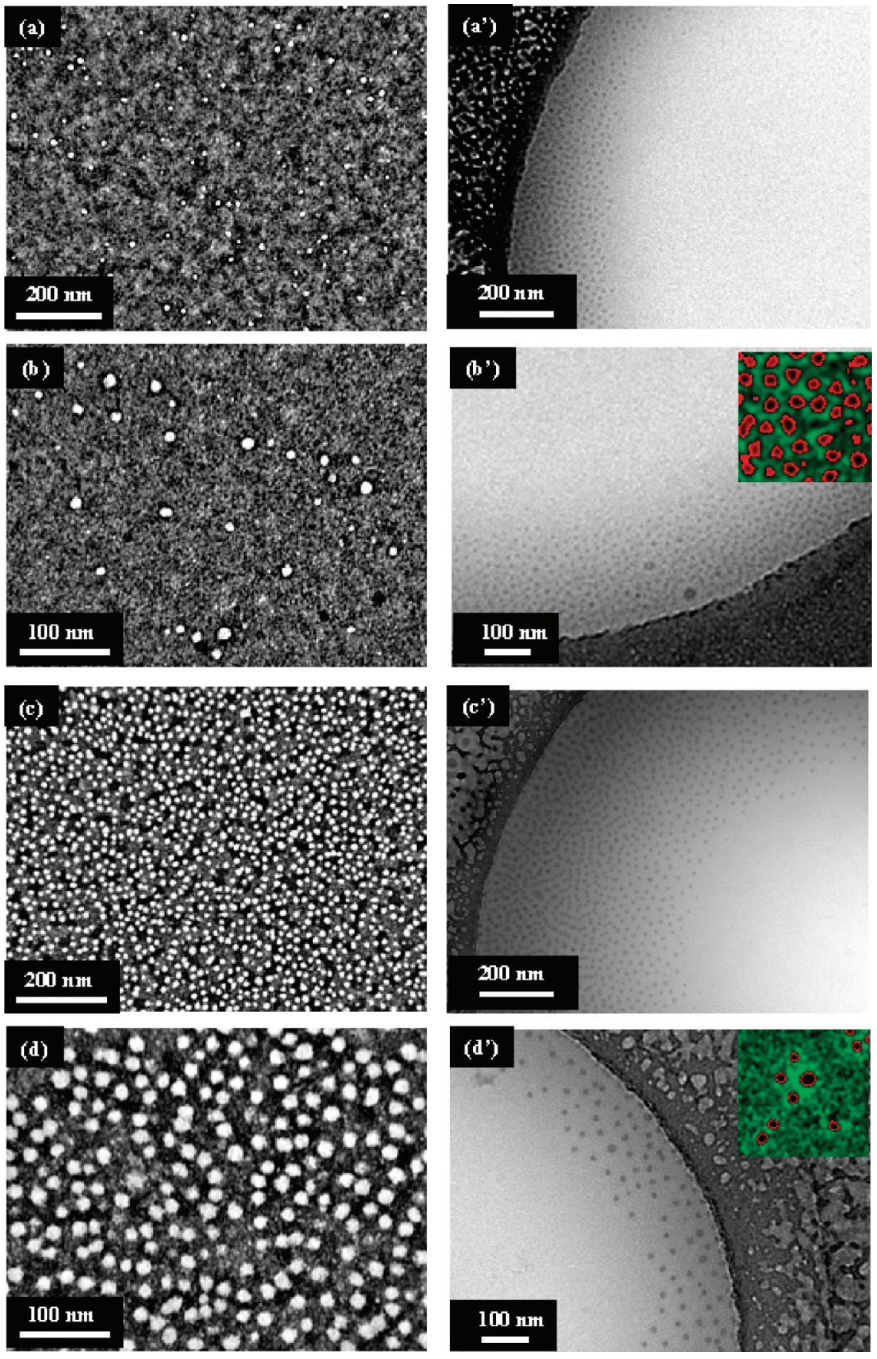

Figure 12. TEM (a-d) and cryo-TEM (a′−d′) of PEO-*b*-PEA$_{10}$ and PEO-*b*-PEA$_{25}$: (a, b) negatively stained TEM of PEO-*b*-PEA$_{10}$; (a′, b′) vitreous thin film cryo-TEM from an aqueous dispersion of PEO-*b*-PEA$_{10}$ and in the inset of part b′ the corresponding false-color contrast-enhancing of a higher magnification zone; (c, d) negatively stained TEM of PEO-*b*-PEA$_{25}$; (c′−d′) Vitreous thin film cryo-TEM from an aqueous dispersion of PEO-*b*-PEA$_{25}$ and in the inset of part d′ the corresponding false-color contrast-enhancing of a higher magnification zone.

For the PEO-*b*-PEA$_{10}$, a value of 2.3 nm is expected for a PEA bulky core radius. The experimental value ($R_{\text{core}} = R_{h\text{micelle}} - \delta_{\text{corona}}$) was 3.6 nm. So, the PEA core volume is about 4 times larger than expected. The same comparison was made with PEO-*b*-PEA$_{17}$ compared to PEO-C$_{22}$ (Renou et al.), both giving an aggregation number around 60, and an excess volume of the core was also found. We concluded that the PEA core is not completely hydrophobic and that it is hydrated. A few years ago, Wu and Gao developed a simple scaling model that predicts a linear dependence of the inverse of the core radius with the inverse of the number of solvophobic units:[69] $R_{core}^{-1} \propto N_B^{-1}$. It would be helpful to check whether PEA cores follow this relation, unfortunately, DLS cannot provide precise data on the micelle core size. Some poly(alkylene oxide) based block copolymers are well-known to form hydrated micellar cores in water. For example, small angle neutron scattering (SANS) experiments on PEO-*b*-PPO-*b*-PEO block copolymers have shown water contents from 5% to 63% in the PPO cores.[70−72] PEO-*b*-PBO copolymers have also been studied by SANS and the hydration of the PBO cores was found to vary from 40% to 67%.[73,74] To our knowledge, it is the first time that a PEO-*b*-poly(alkyl acrylate) amphiphilic block copolymer exhibits a water uptake from the hydrophobic core. However, the error made on the hydrodynamic radius measurements is too large to lead a reliable systematic study on the degree of

hydration by light scattering. Pyrene fluorescence measurements could have brought indications on the water uptake of the core for pyrene fluorescence is known to be affected by the polarity, unfortunately, the experimental errors on the determination of the ratio $I_{336.5}/I_{333.5}$ (excitation) or I_3/I_1 (emission) are too large to conclude on the polarity probed by the pyrene. Small angle X-ray scattering (SAXS) measurements are in progress to confirm the observations made by DLS and SANS measurements could allow the determination of the hydration rate of the micelle cores if this hypothesis is verified.

2.3. Influence of Temperature on Copolymer Micellization. The temperature dependence of the self-associating properties of PEO-*b*-PEA copolymers was studied by SLS between 20 and 80 °C in dilute solution (2.6 g L^{-1}). Figure 10 shows the evolution of the apparent molar mass of the micelles at the temperature (T) divided by its value at 20 °C ($M_{app}(T)/M_{app}(20\ °C)$) as a function of the temperature (T). This figure exhibits an increase of the micelles molar mass as the temperature increases. The slope of $M_{app}(T)/M_{app}(20\ °C) = f(T)$ depends on the PEA block length. The smaller is the hydrophobic block, the higher is the relative molar mass increase. We point out that the variation of the micelles molar mass is totally reversible and reproducible. This suggests that these copolymer micelles are in a thermodynamic equilibrium at all the temperatures studied.

An increase of the aggregation number as a function of temperature has already been shown for PEO-*b*-PPO,[70−72,75−78] PEO-*b*-PBO[73,74,79] and PEO-*b*-PSO[80] block copolymers in aqueous solution and for PS-*b*-PtBuS in *N*, *N*-dimethylacetamide.[81] This phenomenon has been attributed to an enhancement of the core hydrophobicity due to a dehydration of this one. Indeed, when increasing the temperature, water becomes progressively a worse solvent for both the PEO and the hydrophobic block. We strongly believe that the same phenomenon occurs with PEO-*b*-PEA.

The apparent hydrodynamic radius remains almost constant within the experimental error (see Figure 11). A slight increase of R_h is observed for the copolymers bearing the smallest PEA blocks, but the increase does not exceed 10%. This volume increase can be explained by the increase of the number of arms per micelles (N_{agg}). A model of star polymers developed by Daoud and Cotton[82] predicts a power law dependence of the star radius with number of arms with an exponent of 0.2. In the case of copolymer micelles, the following expression can be written: $R_h \sim N_{agg}^{0.2}$. Thus, increasing the aggregation number by 50% only induces an increase of R_h of 8%. The experimental results are in agreement with this prediction.

2.4. Electron Microscopy Analysis. Morphology and size of the copolymer micelles were investigated by transmission electron microscopy (TEM) after negative staining using uranyl acetate and cryo-TEM from aqueous vitreous thin film. Two copolymers with different PEA block lengths (10 and 25 EA units) were visualized by these techniques (see Figure 12). Both TEM and cryo-TEM show nanosized spherical objects and a relatively narrow polydispersity of the micelles diameters. Indeed, in the negatively stained TEM experiments, the whole micelles are surrounded by the uranyl salts and the whiter particles that can be seen corresponds to both the core and the shell. The cryo-TEM experiments have the advantage to avoid any drying step of the aqueous part or staining with heavy metals, and the morphology and size are expected to be as similar as possible than they exist in the aqueous environment. The contrast

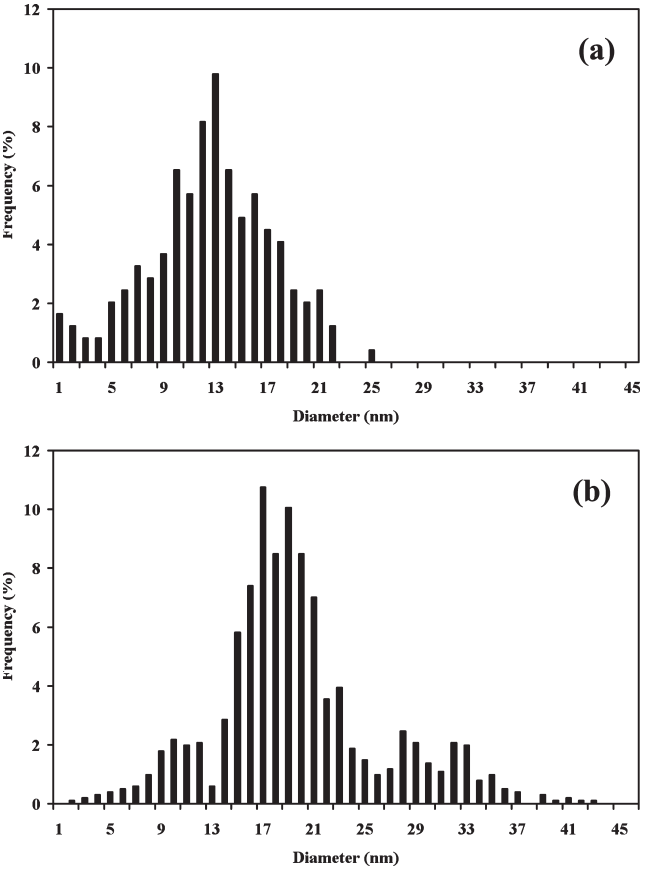

Figure 13. Particle size distributions of (a) PEO-*b*-PEA10 and (b) and PEO-*b*-PEA25 deduced from negatively stained TEM image analysis. The mean diameter and square root are for, respectively, PEO-*b*-PEA10 and PEO-*b*-PEA25 of 12.5 and 4 nm and of 18.6 and 6.5 nm.

of the particles appearing in the cryo-TEM images is also inverse as compared with the negatively stained images. The whole particle contrast is darker than the surrounding solid water and appears with a spherical shape. Cryo-TEM micrographs show undoubtedly a spherical core−shell structure, even for large aggregation numbers, as can be seen on the higher magnification views of Figure 12, parts b′ and d′. The shell that has a weaker apparent density is designed as a diffuse ring with a low contrast, compatible with a high degree of swelling. The cores appear darker than the corona because of their denser electron density. When a contrast enhancement was applied on magnification zones of the cryo-TEM images, and converting the natural apparent contrasts of both core and shell to false colors (black and red), the core−shell morphology of the PEO-*b*-PEA_{10} and PEO-*b*-PEA_{25} particles is evidenced (see the inset of Figure 12, parts b′ and d′).

Figure 13 shows the particle size distributions of PEO-*b*-PEA_{10} (Figure 13a) and PEO-*b*-PEA_{25} (Figure 13b) that has been established by counting more than 200 particles from negatively stained TEM images. The mean diameters deduced from the histograms are found to be of 12.5 and 18.6 nm for, respectively, PEO-*b*-PEA_{10} and PEO-*b*-PEA_{25}. An estimation of the dimension of both the core and shell had also been checked from the higher magnification views of the cryo-TEM images, after enhancing the contrast using the ImageJ software. The diameter of the cores ranges from 4 to 6 nm and 10 to 14 nm for, respectively, PEO-*b*-PEA_{10} and PEO-*b*-PEA_{25}. The thickness of the corona ranges from 1 to 4 nm and from 4 to 8 nm for, respectively, PEO-*b*-PEA_{10} and PEO-*b*-PEA_{25}.

Conclusion

Amphiphilic block copolymers of poly(ethyl acrylate) were synthesized by ATRP using a PEO macroinitiator and either PMDETA or Me_6TREN as ligands. Both catalytic systems ($Cu^{(I)}Br$/PMDETA and Cu(I)Br/Me_6TREN) produces PEO-*b*-PEA block copolymers with predetermined molecular weights and low polydispersity indexes (PDI < 1.1). Several well-defined block copolymers with PEA/PEO molar ratios ranging from 4/96 to 23/77 were successfully synthesized. Their self-assembly behavior in aqueous solution was deeply studied using a large number of techniques. Critical micelle concentrations determined by fluorescence measurements decrease from 0.15 to 0.003 g L^{-1} when the polymerization degrees of EA increase from 8 to 25. Aggregation numbers (N_{agg}), hydrodynamic radii (R_h) and core radii (R_{core}) determined by SLS, DLS and cryo-TEM respectively show an increase with an increase of polymerization degrees of EA. Different ways of preparing samples lead to the same N_{agg} and R_h indicating a fast equilibration process due to the dynamical character of the self-assembly. A temperature increase induces an augmentation of the aggregation number. This effect could be explained by the dehydration of partially solvated micelles cores. This variation of N_{agg} is fully reversible, confirming the fast dynamics of the PEO-*b*-PEA micellar system. These copolymers can be functionalized at the end of the PEA block. A methacrylate group will be introduced at the end of the hydrophobic block and the self-assembled structures will be rapidly cross-linked under UV irradiation. The functionalization and the cross-linking studies will be the objet of a future paper.

Acknowledgment. The authors thank the Région des Pays de la Loire and the National Research Agency (ANR) for their financial support, Jean-Claude Soutif for MALDI−TOF measurements and Taco Nicolai for the fruitful discussions.

References and Notes

(1) Alexandridis, P.; Lindman, B., *Amphiphilic Block copolymers*. Elsevier: Amsterdam, **2000**.
(2) Hamley, I. W., Block copolymers in dilute solution. In *The Physics of Block Copolymers*, Hamley, I. W., Ed. Oxford University Press: Oxford, U.K., **1998**; pp 131−220.
(3) Antonietti, M.; Förster, S. *Adv. Mater*. **2003**, *15*, 1323–1333.
(4) Discher, D. E.; Eisenberg, A. *Science* **2002**, *297*, 967–973.
(5) Lim Soo, P.; Eisenberg, A. *J. Polym. Sci., Part B: Polym. Phys*. **2004**, *42*, 923–938.
(6) Maskos, M.; Harris, J. R. *Macromol. Rapid Commun*. **2001**, *22*, 271–273.
(7) Zhang, L.; Eisenberg, A. *Science* **1995**, *268*, 1728–1731.
(8) Riess, G. *Prog. Polym. Sci*. **2003**, *28*, 1107–1170.
(9) Otsuka, H.; Nagasaki, Y.; Kataoka, K. *Curr. Opin. Colloid Interface Sci*. **2001**, *6*, 3–10.
(10) Alexandridis, P.; Hatton, T. A. *Colloids Surf. A: Phys. Eng. Asp*. **1995**, *96*, 1–46.
(11) Mortensen, K.; Brown, W.; Jorgensen, E. *Macromolecules* **1994**, *27*, 5654–5666.
(12) Lang, M.; Zhang, G.; Feng, N.; Li, S.; Chen, X. *J. Appl. Polym. Sci*. **1997**, *65*, 1667–1674.
(13) Wang, J.; Varshney, S. K.; Jerome, R. *J. Polym. Sci., Part A: Polym. Chem*. **1992**, *30*, 2251–2261.
(14) Kamigaito, M.; Ando, T.; Sawamoto, M. *Chem. Rev*. **2001**, *101*, 3689–3746.
(15) Matyjaszewski, K.; Xia, J. *Chem. Rev*. **2001**, *101*, 2921–2990.
(16) Dai, S.; Ravi, P.; Leong, C. Y.; Tam, K. C.; Gan, L. H. *Langmuir* **2004**, *20*, 1597–1604.
(17) Ranger, M.; Jones, M.-C.; Yessine, M.-A.; Leroux, J.-C. *J. Polym. Sci., Part A: Polym. Chem*. **2001**, *39*, 3861–3874.
(18) Sant, V. P.; Smith, D.; Leroux, J.-C. *J. Contr. Release* **2004**, *97*, 301–312.
(19) Bednarek, M.; Biedron, T.; Kubisa, P. *Macromol. Rapid Commun*. **1999**, *20*, 59–65.
(20) Ma, Z.; Lacroix-Desmazes, P. *Polymer* **2004**, *45*, 6789–6797.
(21) Hou, S.; Chaikof, E. L.; Taton, D.; Gnanou, Y. *Macromolecules* **2003**, *36*, 3874–3881.
(22) Kul, D.; Van Renterghem, L. M.; Meier, M. A. R.; Strandman, S.; Tenhu, H.; Yilmaz, S. S.; Schubert, U. S.; Du Prez, F. E. *J. Polym. Sci., Part A: Polym. Chem*. **2008**, *46*, 650–660.
(23) Durmaz, H.; Karatas, F.; Tunca, U.; Hizal, G. *J. Polym. Sci., Part A: Polym. Chem*. **2006**, *44*, 3947–3957.
(24) Rodríguez-Hernández, J.; Chécot, F.; Gnanou, Y.; Lecommandoux, S. *Prog. Polym. Sci*. **2005**, *30*, 691–724.
(25) O'Reilly, R. K.; Hawker, C. J.; Wooley, K. L. *Chem. Soc. Rev*. **2006**, *35*, 1068–1083.
(26) Nicol, E.; Niepceron, F.; Bonnans-Plaisance, C.; Durand, D. *Polymer* **2005**, *46*, 2020–2028.
(27) Ciampolini, M.; Nardi, N. *Inorg. Chem*. **1966**, *5*, 41–44.
(28) Wilhelm, M.; Zhao, C.-L.; Wang, Y.; Xu, R.; Winnik, M. A.; Mura, J.-L.; Riess, G.; Croucher, M. D. *Macromolecules* **1991**, *24*, 1033–1040.
(29) Brown, W., *Light Scattering. Principles and Developments*; Clarendon Press: Oxford, U.K., **1996**.
(30) Higgins, J. S.; Benoit, K. C., *Polymer and Neutron Scattering*; Clarendon Press: Oxford, **1994**.
(31) Xu, R.; Winnik, M. A.; Hallett, F. R.; Riess, G.; Croucher, M. D. *Macromolecules* **1991**, *24*, 97–93.
(32) Michielsen, S. Specific index increments of polymers in dilute solution. In *Polymer Handbook*, 4th ed., Brandrup, J. I., E. H.; Grulke, E. A., Eds.; John Wiley and Sons, Inc.: New-York, **1999**; pp 594-595.
(33) Wesslau, H. *Makromol. Chem*. **1963**, *69*, 213–219.
(34) Berne, B.; Percora, R., *Dynamic Light Scattering*; Wiley: New York, **1976**.
(35) Brown, W., *Dynamic Light Scattering. The Method and Some Applications*. Clarendon Press: Oxford, U.K., **1993**.
(36) Xia, J.; Matyjaszewski, K. *Macromolecules* **1997**, *30*, 7697–7700.
(37) Xia, J.; Gaynor, G.; Matyjaszewski, K. *Macromolecules* **1998**, *31*, 5958–5959.
(38) Tang, W.; Matyjaszewski, K. *Macromolecules* **2006**, *39*, 4953–4959.
(39) Kalyanasundaram, K.; Thomas, J. K. *J. Am. Chem. Soc*. **1977**, *99*, 2039–2044.
(40) Aguiar, J.; Carpena, P.; Molina-Bolivar, J. A.; Carnero Ruiz, C. *J. Colloid Interface Sci*. **2003**, *258*, 116–122.
(41) Astafieva, I.; Zhong, X. F.; Eisenberg, A. *Macromolecules* **1993**, *26*, 7339–7352.
(42) Cheon, J.-B.; Jeong, Y.-I.; Cho, C.-S. *Polymer* **1999**, *40*, 2041–2050.
(43) Inoue, T.; Chen, G.; Nakamae, K.; Hoffman, A. S. *J. Controlled Release* **1998**, *51*, 221–229.
(44) Jeong, Y.-I.; Cheon, J.-B.; Kim, S.-H.; Nah, J.-W.; Lee, Y.-M.; Sung, Y.-K.; Akaike, T.; Cho, S.-C. *J. Controlled Release* **1998**, *51*, 169–178.
(45) Lee, R.-S.; Li, H.-L.; Yang, J.-M.; Tsai, F.-Y. *Polymer* **2005**, *46*, 10718–10726.
(46) Kwon, G.; Naito, M.; Yokoyama, M.; Okano, T.; Sakurai, Y.; Kataoka, K. *Langmuir* **1993**, *9*, 945–949.
(47) Nivaggioli, T.; Alexandridis, P.; Hatton, T. A.; Yekta, Y.; Winnik, M. A. *Langmuir* **1995**, *11*, 730–737.
(48) Wang, D.; Peng, Z.; Liu, X.; Tong, Z.; Wang, C.; Ren, B. *Eur. Polym. J*. **2007**, *43*, 2799–2808.
(49) Zhao, C.-L.; Winnik, M. A. *Langmuir* **1990**, *6*, 514–516.
(50) Narrainen, A. P.; Pascual, S.; Haddleton, D. M. *J. Polym. Sci., Part A: Polym. Chem*. **2002**, *40*, 469–450.
(51) Anthony, O.; Zana, R. *Macromolecules* **1994**, *27*, 3885–3891.
(52) Booth, C.; Attwood, D.; Price, C. *Phys. Chem. Chem. Phys*. **2006**, *8*, 3612–3622.
(53) Khougaz, K.; Zhong, X. F.; Eisenberg, A. *Macromolecules* **1996**, *29*, 3937–3949.
(54) Colombani, O.; Ruppel, M.; Burkhardt, M.; Drechsler, M.; Schumacher, M.; Gradzielski, M.; Schweins, R.; Muller, A. H. E. *Macromolecules* **2007**, *40*, 4351–4362.
(55) Jacquin, M.; Muller, P.; Talingting-Pabalan, R.; Cottet, H.; Berret, J. F.; Futterer, T.; Théodoly, O. *J. Colloid Interface Sci*. **2007**, *316*, 897–911.
(56) Bendejacq, D. D.; Ponsinet, V.; Joanicot, M. *Langmuir* **2005**, *21*, 1712–1718.
(57) Choucair, A.; Kycia, A. H.; Eisenberg, A. *Langmuir* **2003**, *19*, 1001–1008.
(58) Shen, H.; Eisenberg, A. *J. Phys. Chem. B* **1999**, *103*, 9473–9487.
(59) Annable, T.; Buscall, R.; Ettelaie, R.; Whittlestone, D. *J. Rheol*. **1993**, *37*, 695–725.
(60) Berret, J.-F.; Calvet, D.; Collet, A.; Viguier, M. *Curr. Opin. Colloid Interface Sci*. **2003**, *8*, 296–306.

(61) Halperin, A. *Macromolecules* **1987**, *20*, 2943–2946.
(62) Noolandi, J.; Hong, K. M. *Macromolecules* **1983**, *16*, 1443–1448.
(63) Nagarajan, R.; Ganesh, K. *J. Chem. Phys.* **1989**, *90*, 5843–5856.
(64) Booth, C.; Attwood, D. *Macromol. Rapid Commun.* **2000**, *21*, 501–527.
(65) Antonietti, M.; Heinz, S.; Schmidt, M.; Rosenauer, C. *Macromolecules* **1994**, *27*, 3276–3281.
(66) Förster, S.; Zisenis, M.; Wenz, E.; Antonietti, M. *J. Chem. Phys.* **1996**, *104* (24), 9956–9970.
(67) Qin, A.; Minmin, T.; Ramireddy, C.; Webber, S. E.; Munk, P. *Macromolecules* **1994**, *27*, 120–126.
(68) Renou, F.; Nicolai, T.; Nicol, E.; Benyahia, L. *Langmuir* **2009**, *25*, 515–521.
(69) Wu, C.; Gao, J. *Macromolecules* **2000**, *33*, 645–646.
(70) Goldmints, I.; von Gottberg, F. K.; Smith, K. A.; Hatton, T. A. *Langmuir* **1997**, *13*, 3659–3664.
(71) Goldmints, I.; Yu, G.-E.; Booth, C.; Smith, K. A.; Hatton, T. A. *Langmuir* **1999**, *15*, 1651–1656.
(72) Liu, Y.; Chen, S.-H.; Huang, J. S. *Macromolecules* **1998**, *31*, 2236–2244.
(73) Derici, L.; Ledger, S.; Mai, S.-M.; Booth, C.; Hamley, I. W.; Pedersen, J. S. *Phys. Chem. Chem. Phys.* **1999**, *1*, 2773–2785.
(74) Castelletto, V.; Hamley, I. W. *Langmuir* **2004**, *20*, 2992–2994.
(75) Wanka, G.; Hoffmann, H.; Ulbricht, W. *Macromolecules* **1994**, *27*, 4145–4159.
(76) Altinok, H.; Nixon, S. K.; Gorry, P. A.; Attwood, D.; Booth, C.; Kelarakis, A.; Havredaki, V. *Coll. Surf. B: Biointerfaces* **1999**, *16*, 73–91.
(77) Kelarakis, A.; Yang, Z.; Pousia, E.; Nixon, S. K.; Price, C.; Booth, C.; Hamley, I. W.; Castelletto, V.; J., F. *Langmuir* **2001**, *17*, 8085–8091.
(78) Yang, L.; Alexandridis, P.; Steytler, D. C.; Kositza, M. J.; Holzwarth, J. F. *Langmuir* **2000**, *16*, 8555–8561.
(79) Mingvanish, W.; Mai, S.-M.; Heatley, F.; Booth, C. *J. Phys. Chem. B* **1999**, *103*, 11269–11274.
(80) Mai, S.; Booth, C.; Kelarakis, A.; Havredaki, V.; Ryan, A. J. *Langmuir* **2000**, *16*, 1681–1688.
(81) Zhou, Z.; Chu, B.; Peiffer, D. G. *Macromolecules* **1993**, *26*, 1876–1883.
(82) Daoud, M.; Cotton, J.-P. *J. Phys. (Paris)* **1982**, *43*, 531–538.